

**Electronic Supporting Information (ESI)**

**Ballistic  $\Delta S=2$  Intersystem Crossing in a Cobalt Cubane Following Ligand-Field Excitation  
Probed by Extreme Ultraviolet Spectroscopy**

Yusef Shari'ati and Josh Vura-Weis

Department of Chemistry, University of Illinois at Urbana-Champaign, IL, USA

**Contents**

1. Materials & Sample Preparation .....	1
2. M-edge XANES Spectroscopy .....	2
3. Kinetic Modeling & Global Analysis .....	5
4. Tanabe-Sugano Diagram.....	9
5. Ligand Field Multiplet Simulations .....	10
6. DFT Summary.....	11
7. DFT Geometries .....	11
8. References .....	16

**1. Materials & Sample Preparation**

Cobalt cubane was synthesized according to literature procedures<sup>1</sup>, using cobalt(II) acetate tetrahydrate in lieu of cobalt nitrate and sodium acetate. The UV-visible spectrum of cobalt cubane in dichloromethane is shown in Figure S1.

Thin film samples were prepared in a manner described previously.<sup>2</sup> Specifically, films were spin-coated from 25 mM cubane in mixed alcohol solution (4 parts methanol, 2 parts isopropyl alcohol, and 1 part butanol, by mass) at 1500 rpm onto 185 nm thin films of poly(vinyl)chloride (PVC,  $M_w = 275,000$ , Scientific Polymer Products Inc.). The PVC films had been previously deposited in the same way from 2.5% w/w cyclohexanone solution on clean glass slides. The films were delaminated over water and thicknesses determined from UV-Visible spectroscopy. Under these conditions, ~200 nm of cubane film is deposited upon the PVC. Sample films are mounted on 525  $\mu\text{m}$  thick 7.5×7.5 mm silicon frames (Silson Ltd.), with a central open window of 2×2 mm.

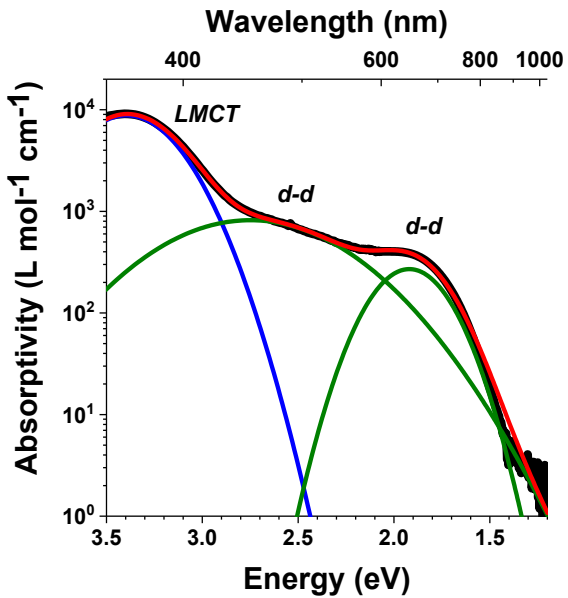


**Figure S1.** UV-Visible spectrum of  $\text{Co}_4\text{O}_4$  in dichloromethane (black), decomposed into three gaussians (blue and green) whose sum is shown in red.

## 2. M-edge XANES Spectroscopy

**Instrument.** The extreme ultraviolet (XUV) probe is generated via high-harmonic generation (HHG) in an instrument described previously.<sup>3</sup> A Ti:sapphire laser (Spectra-Physics Spitsfire Ace) produces 6 mJ pulses of 800 nm light at 1 kHz repetition rate with a pulse width of 35 fs FWHM. 4 mJ of this source is focused into a semi-infinite gas cell containing neon gas at ~100 torr. Residual IR is removed with a Si mirror, followed by a 100 nm Al filter. The XUV continuum so produced has intensity in the range 40-90 eV, as shown in Figure S2, and is detected by a CCD (Oxford Instruments ANDOR, model Newton DO920P-BEN) cooled to -60°C. Calibration of the XUV spectrometer is performed daily by measuring the Al L-edge at 72.64 eV,<sup>4</sup> ionized Xe,<sup>5</sup> the  $M_{2,3}$ -edge peaks of  $\text{Fe}_2\text{O}_3$  at 57.5 eV,<sup>4</sup> and NiO at 66.3 eV.<sup>6,7</sup> The instrumental energy resolution is calculated from the spectral width of the sharp lines of ionized xenon, here measured as 0.3 eV FWHM.

**Ground State Data Collection.** Ground state spectra were acquired by referencing sample films to 185 nm PVC membrane. Absorbance values are computed from the base-10 logarithm of ratio between sample and reference counts detected at the CCD. Ground state spectra are reported after power-law subtraction, which removes non-resonant signal from photoionization of valence electrons. The power law is shown in equation (1). The constant  $\alpha$  is proportional to the thickness of the sample,  $E$  is the energy in electron-volts, and the constant exponent  $b$  relates to the atomic composition of the sample.  $E_0$  is taken to be 1 eV here to ensure a unitless result. For the purposes of subtraction, constants are empirically derived from a fit to the flat region (54-60 eV) prior to onset of the cobalt edge (Figure S3).

$$A(E) = \alpha \left( \frac{E}{E_0} \right)^{-b} \quad (1)$$

**Transient Data Collection.** The 550 nm pump for transient experiments is produced by diverting a 0.65 mJ portion of the Ti:sapphire beam to a noncollinear optical parametric amplifier (TOPAS White). The pump and probe sizes were measured at the sample via knife-edge scans; the XUV probe beam size was 75  $\mu\text{m}$  FWHM and the pump was 180  $\mu\text{m}$  FWHM. Cubane samples had an absorbance of 0.03 at 550 nm, and were photoexcited at 2.5 mJ/cm<sup>2</sup> yielding a calculated 4% sample excitation fraction per pulse.

Temporal overlap between the pump and XUV probe was attained by measuring the onset of the transient bleach signal from Fe<sub>2</sub>O<sub>3</sub> samples between 57 and 58 eV.<sup>4</sup> Time zero was found to drift  $\pm 35$  fs over an  $\sim$ 10-hour period; this has been corrected for by periodically repeating the temporal overlap measurement of Fe<sub>2</sub>O<sub>3</sub> every 2-3 hours. Plotted in Figure S4 are the Fe<sub>2</sub>O<sub>3</sub> data along with the early time cubane data, showing a clear delay in the cubane transient response.

A stream of low-pressure nitrogen gas was passed across all samples to mitigate pump-induced heating and/or damage. The transient XUV experiment ran a total of 23 hours, divided equally over three  $\sim$ 4 mm<sup>2</sup> cubane samples. Samples were rastered in 50  $\mu\text{m}$  steps such that each step received no more than a cumulative  $\sim$ 30 s of pump and probe exposure. As shown in Figure S5, no sample damage is detected.

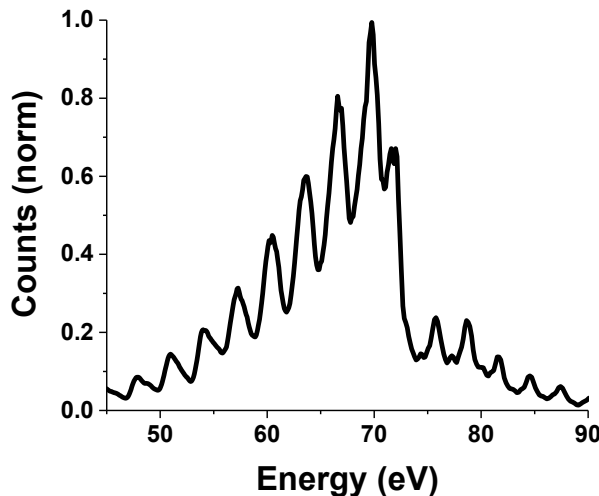


**Figure S2.** The XUV probe continuum generated via HHG in  $\sim$ 100 torr neon gas.

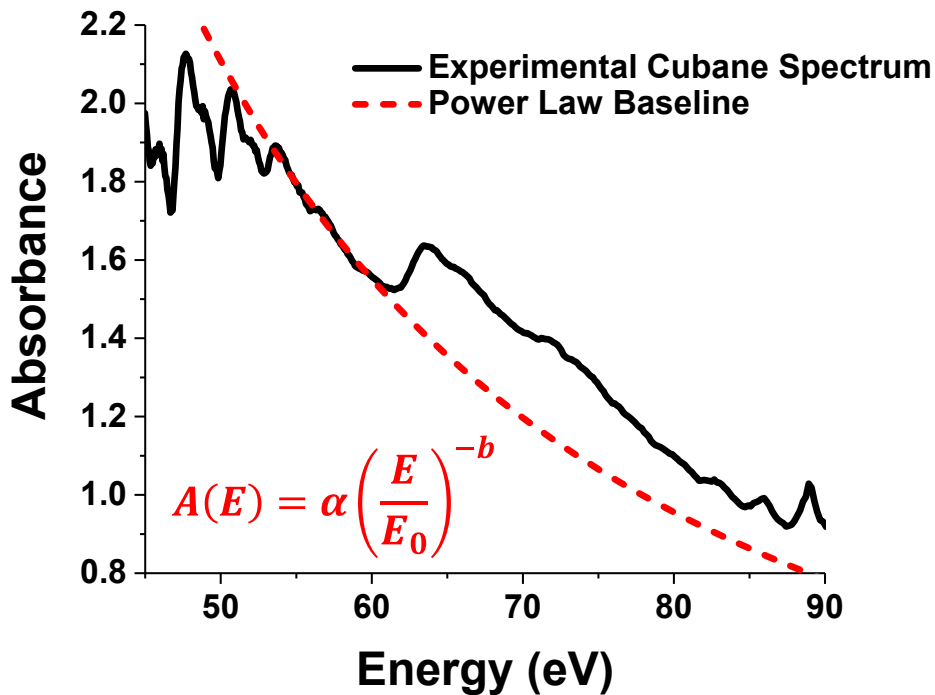


**Figure S3.** Spectrum of cubane before baseline subtraction (black solid line), with power law fit (red dashed line). Fit parameters are:  $\alpha = 1.56 \times 10^3$ ,  $b = 1.68$ ,  $E_0 = 1$  eV. The cobalt edge appears near 63 eV, while the sharp deviations from the power law below 55 eV and above 80 eV are due to low probe continuum counts in those regions.

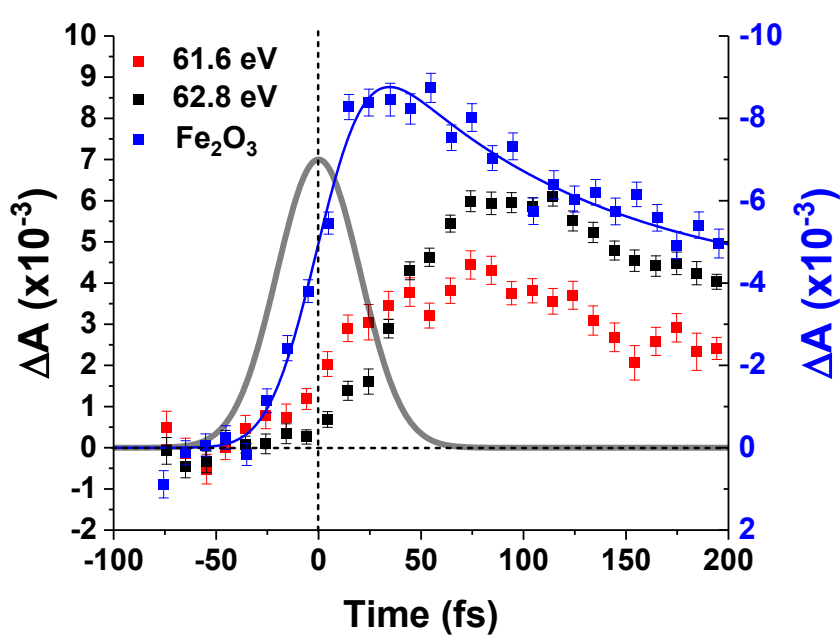


**Figure S4.** Early time cubane data and the IRF limited signal from  $\text{Fe}_2\text{O}_3$  is plotted with its corresponding fit in blue. Error bars correspond to  $\pm$  the standard error. A gaussian profile corresponding to the 48 fs time resolution is plotted in grey.

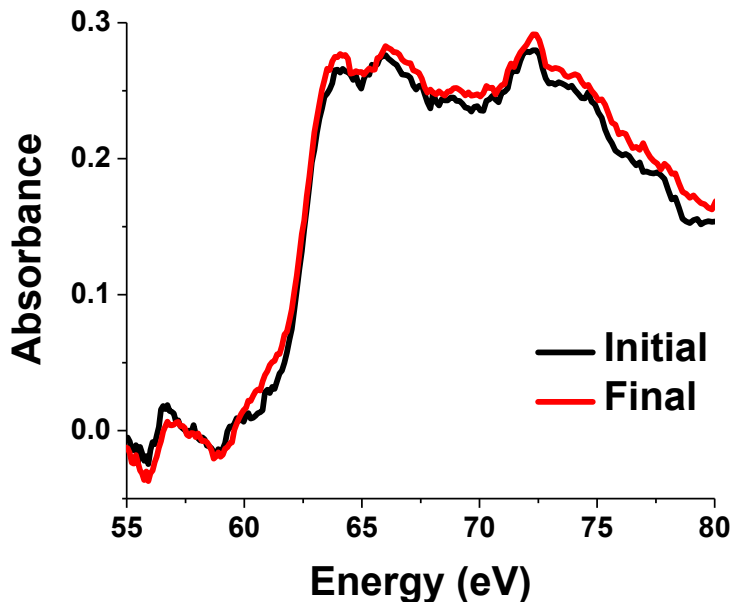
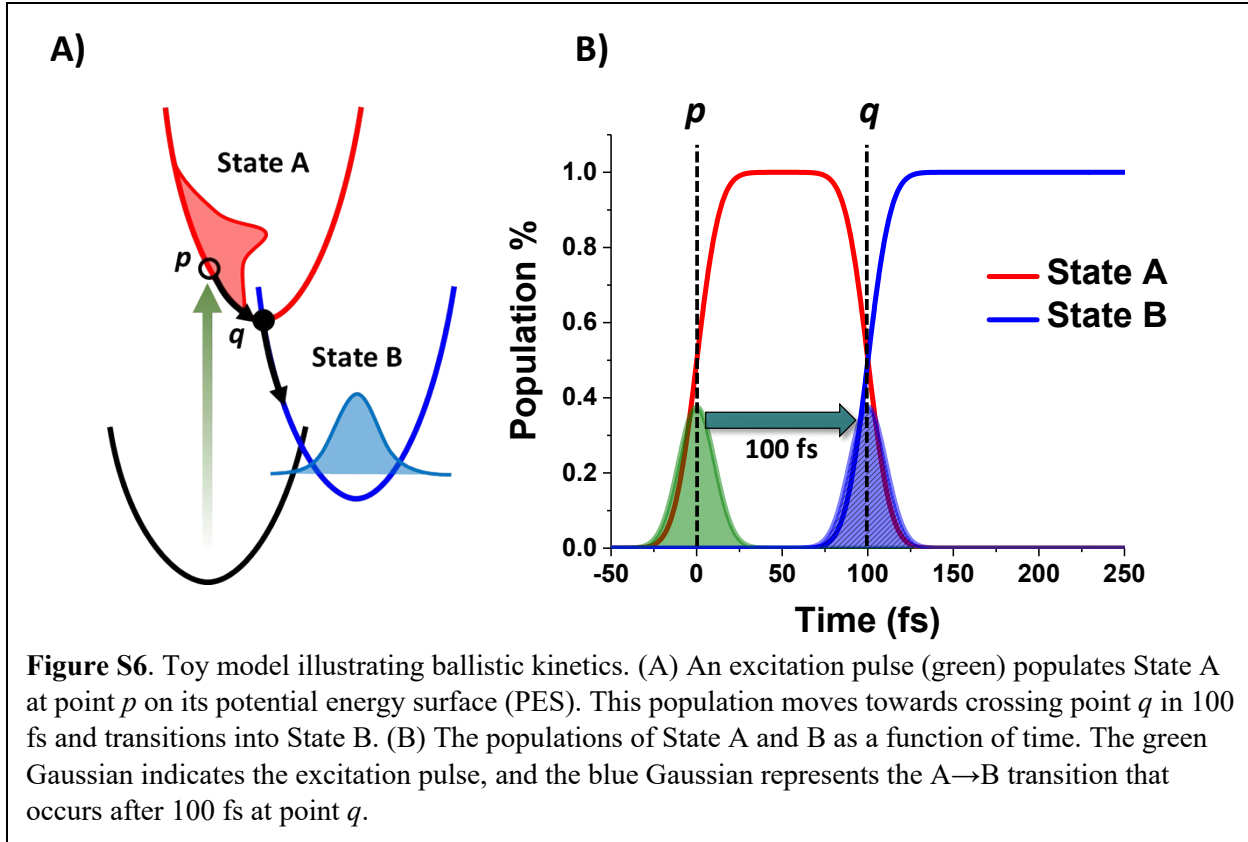


**Figure S5.** Ground state  $M_{2,3}$ -edge XANES spectrum of a typical cubane sample before (black trace) and after  $\sim 8$  hours of rastered data collection (red trace). No sample damage is indicated.

### 3. Kinetic Modeling & Global Analysis

Exponential kinetics arise when the transitions between states derive from the probabilistic overtopping of a reaction barrier between those states, with the barrier height described by the activation energy. “Ballistic” kinetics instead arise when a population moves as a coherent unit through an essentially barrierless crossing on the potential energy surface. In such systems, the inappropriate application of exponential kinetics fails to capture the dynamics correctly. Figure S6A depicts a toy model of a three-state system in which a population is excited into State A at point  $p$  on its potential energy surface (PES) at time zero by a Gaussian (in time) pulse, here 25 fs FWHM. The non-equilibrium population evolves following nuclear motion towards the curve minimum, following a classical trajectory on the PES. Crossing point  $q$  is reached after a travel time of 100 fs and the population moves into State B with 100% efficiency. When the barrier is non-zero sub-unity crossing efficiency occurs and with further increases of barrier height the kinetics become increasingly probabilistic. State B undergoes no further evolution in the timescale of this toy model. Figure S6B shows a numerical simulation of the populations as a function of time. Unlike exponential kinetics the population of State A remains constant for a time then falls abruptly, moderated by the IRF. Note that a slow IRF precludes observation of this behavior and hinders discrimination between exponential and ballistic kinetics. Similarly, long travel times on the PES may permit decoherence of the population and begin to favor exponential dynamics.



The functional form of the population of State A is shown in equation (2), where  $t$  is time,  $\sigma$  is the Gaussian width, and  $\omega$  is the travel time between points  $p$  and  $q$ :

$$A(t) = \frac{1}{2} \left[ \text{erf}\left(\frac{t}{\sqrt{2}\sigma}\right) - \text{erf}\left(\frac{t-\omega}{\sqrt{2}\sigma}\right) \right] \quad (2)$$

The horizontal shift in the function corresponds physically to the time of the transition event, i.e. the time when the crossing point on the potential energy surface is encountered.

#### 4. Fit Parameters & Uncertainty Characterization

To mitigate biasing the results, fitting was repeated 25 times with initial fit parameters for the global analysis randomly sampled from a uniform distribution within the ranges indicated in Table S1. The resultant fit parameters are robust to this variation and consistently converge to the same values (reported) with less than 0.1% standard deviation.

	Range
$\omega_1/\tau_1$	20 – 60 fs
$\omega_2/\tau_2$	30 – 200 fs
$\tau_3$	400 fs – 10 ps
$\tau_4$	50 ps – 10 ns

**Table S1.** Ranges of the uniform distributions used for fitting kinetic parameters.

Uncertainties derived from the fitting algorithm do not well relate to uncertainties inherent in the experiment and are, as noted by Zhang *et al*, unphysically small.<sup>8</sup> Therefore, phenomenological uncertainties in the fit parameters were estimated by splitting the data into two equal portions and performing global analysis upon each subset. Effectively equivalent to performing two independent experiments, the resultant different fit parameters (Tables S2 and S3) comprise a basis for estimating the standard error that is reported in the main text, here taken to be sample standard deviation between the two data set fit values ( $\sqrt{2}$  times the difference).

	<b>Full Dataset</b>	<b>Data Subset 1</b>	<b>Data Subset 2</b>
$\tau_1$	29.7 fs	33.7 fs	31.4 fs
$\tau_2$	108 fs	107 fs	81.6 fs
$\tau_3$	2.9 ps	1.76 ps	2.77 ps
$\tau_4$	306 ps	134 ps	296 ps

**Table S2.** Model I fit parameters.

	<b>Full Dataset</b>	<b>Data Subset 1</b>	<b>Data Subset 2</b>
$\omega_1$	38.3 fs	37.5 fs	37.1 fs
$\omega_2$	94.2 fs	98.3 fs	91.5 fs
$\tau_3$	794.0 fs	641 fs	1.13 ps
$\tau_4$	82.6 ps	99.8 ps	120 ps

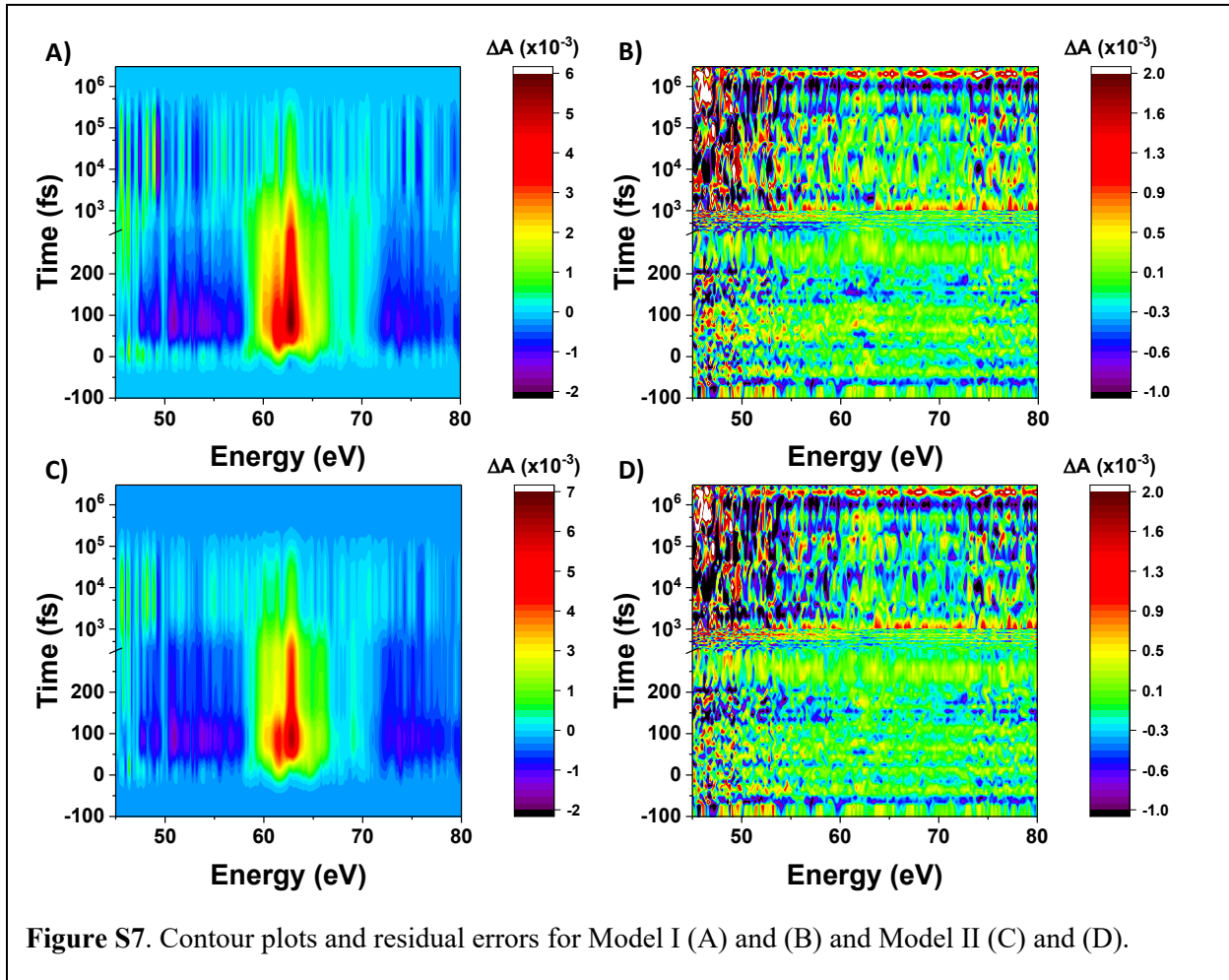
**Table S3.** Model II fit parameters.

### Quantitative Comparison of Models I and II

Contour plots of both models, along with residuals from the global analyses are plotted in Figure S7. A quantitative comparison between Model I and Model II was first accomplished by examining the magnitude of the mean squared errors (MSE), i.e. the mean squared residuals, which are reported in Table S4. Generally, MSE values are comparable in magnitude, though slightly smaller for Model I. If noisier portions of the data set are truncated away (such as the energy range below 50 eV where probe flux is low, or data after 1 ps where error bars are large), then the two models are seen to fit the data almost equally well. Examining the 62.8 eV trace alone (where the decidedly non-exponential kinetics are most apparent) favors Model II with lower MSE values. The significance of the differences between MSE values was evaluated by *z*-test in equation (5), with a *z*-value of 1.96 or greater indicating difference between MSE values, either positively or negatively, at the 95% confidence level. As evidenced by low *z*-values, this simple MSE analysis fails to find any significant difference between models.

	Mean Square Errors	$N$	$z$
	Model I	Model II	
All Data	$(3.44 \pm 0.09) \times 10^{-7}$	$(3.60 \pm 0.09) \times 10^{-7}$	15,312
Data truncated to 50-80 eV, $t < 1$ ps	$(1.23 \pm 0.02) \times 10^{-7}$	$(1.21 \pm 0.02) \times 10^{-7}$	10,117
62.8 eV Trace Only	$(1.05 \pm 0.12) \times 10^{-7}$	$(0.84 \pm 0.09) \times 10^{-7}$	261

**Table S4.** Comparison of mean square errors (MSE) between Models I and II.  $N$  is the number of data points included in the calculation and  $z$  is the test statistic. Errors are  $\pm$  standard error.



### Pairwise Difference Test

While useful as a bird's-eye view of the data, the MSE reductively glosses over correlated differences between the models and thus loses much statistical discriminatory power. In the context of the  $\text{Co}_4\text{O}_4$  transient XUV data, it is evident that Model I fit lines (main text) do not well represent the data as well as Model II, especially the strongest feature (62.8 eV) between 100 and 200 fs. The MSE analysis hides those specific differences by effectively treating them as drawn from a random distribution, when in fact they are correlated. Therefore, average pairwise differences  $D$  for each time point ( $n = 87$ ) were calculated as in equation (3), where  $A_i$  and  $B_i$  are the squared residuals from Model I and Model II at the  $i^{\text{th}}$  data (time) point.

$$D = \frac{1}{n} \sum_{i=1}^n (A_i - B_i) \quad (3)$$

The null hypothesis is  $D = 0$ , that differences between the squared residuals of Model I and II are not significant. To evaluate this, the standard deviation of the differences is computed in (4).

$$\sigma = \sqrt{\frac{\sum_{i=1}^n (D_i - \bar{D})^2}{n}} \quad (4)$$

The test statistic  $Z$  is the quotient in (5), comparing the mean difference  $D$  to its standard deviation of the mean (standard error, where  $n$  is the degrees of freedom). A large  $Z$  indicates that between-group variation ( $\bar{D}$ ) are greater than within-group variation (standard error). Conversely, a small  $Z$  favors the null hypothesis.

$$Z = \frac{D}{\sigma / \sqrt{n}} \quad (5)$$

Now in units of standard deviations,  $Z$  is compared to the standard normal distribution to determine a level of statistical significance. We find, for the 62.8 eV trace that  $D = 2.31 \times 10^{-8}$ ,  $\sigma = 1.13 \times 10^{-7}$  with  $n = 87 - 1$ , and  $Z = 1.89$ . This results in a one-tailed probability of 0.97 that Model II exhibits a smaller squared residual than Model I; we therefore reject the null hypothesis in favor of Model II at the 95% confidence level.

Given the qualitative comparison by visual inspection of the Model I and II fit lines with the data, the quantitative analysis above, and the physical basis for the ballistic kinetics, we prefer Model II as the least parsimonious explanation consistent with the data.

## 5. Tanabe-Sugano Diagram

The ligand-field splitting values of both  $\text{Co}_4\text{O}_4$  cubane and  $\text{Co}(\text{acac})_3$  were estimated using the  $d^6$  Tanabe-Sugano diagram. The experimental UV-visible spectra were measured and corroborated by literature values. Cubane was measured in dichloromethane (Figure S1),<sup>1</sup> and  $\text{Co}(\text{acac})_3$  in toluene (Figure S8).<sup>9</sup> The ratio of the wavelengths of the two lowest allowed transitions ( ${}^1\text{T}_{2g} \leftarrow {}^1\text{A}_{1g}$  and  ${}^1\text{T}_{1g} \leftarrow {}^1\text{A}_{1g}$ ) were used to calculate the Racah parameter  $B$  and the  $10\text{Dq}$  value  $\Delta_0$ . Additionally, energies of the relevant triplet and quintet excited states are predicted. Note that in both cases the lowest energy excited state is predicted to be the  ${}^3\text{T}_{1g}$ . Results are summarized in Table S5.

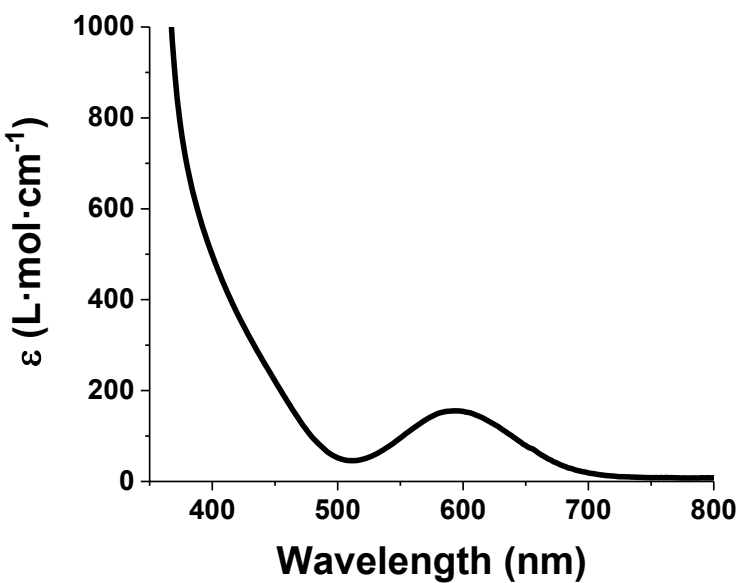


**Figure S8.** The UV-visible spectrum of a 1.26 mM  $\text{Co}(\text{acac})_3$  solution in toluene.

	Cubane	$\text{Co}(\text{acac})_3$
$\nu_1$	650 nm (15,400 $\text{cm}^{-1}$ )	594 nm (16,800 $\text{cm}^{-1}$ )
$\nu_2$	430 nm (23,300 $\text{cm}^{-1}$ )	400 nm (25,000 $\text{cm}^{-1}$ )
$\nu_2/\nu_1$	1.51	1.485
$\Delta_0/B$	27.2	28.9
$E_1/B$	24.5	26.1
B	629 $\text{cm}^{-1}$	648 $\text{cm}^{-1}$
$\Delta_0$	17,100 $\text{cm}^{-1}$ (2.1 eV)	18,700 $\text{cm}^{-1}$ (2.3 eV)
$E(^3\text{T}_{1g})$	1.17 eV	1.33 eV
$E(^5\text{T}_{2g})$	1.30 eV	1.60 eV
$E(^3\text{T}_{2g})$	1.64 eV	1.84 eV

**Table S5.** Parameters for the Tanabe-Sugano diagram calculation of 10Dq for both  $\text{Co}_4\text{O}_4$  cubane and  $\text{Co}(\text{acac})_3$ .

## 6. Ligand Field Multiplet Simulations

LFM simulations were performed with the program CTM4XAS,<sup>10</sup> which we have extended to include variable linewidths (due to state-dependent core-hole lifetimes) and an asymmetric Fano line-shape ( $q=3.5$ ) which arises from interference between Auger decay of the core-hole state and background 3d electron photoionization.<sup>3</sup> The obtained spectral sticks were gaussian broadened with FWHM = 0.2 eV to account for instrumental energy resolution.

Parameters for the cubane simulations were as follows. The crystal-field splitting energy 10Dq was 2.2 eV, while Slater-Condon factor scalings were  $F_{dd} = 1.0$ ,  $F_{pd} = 1.0$ , and  $G_{pd} = 0.825$ . A shift of +60.8

eV was uniformly applied to align spectra with experiment due to systematic inaccuracy of predicted absolute energy values.

Calculations of excited state spectra were performed according to the work of Zhang *et al.*<sup>11</sup> Difference spectra reported in the main text were obtained by subtraction of the corresponding excited state simulation spectrum (Figure S9) from the ground state simulation.

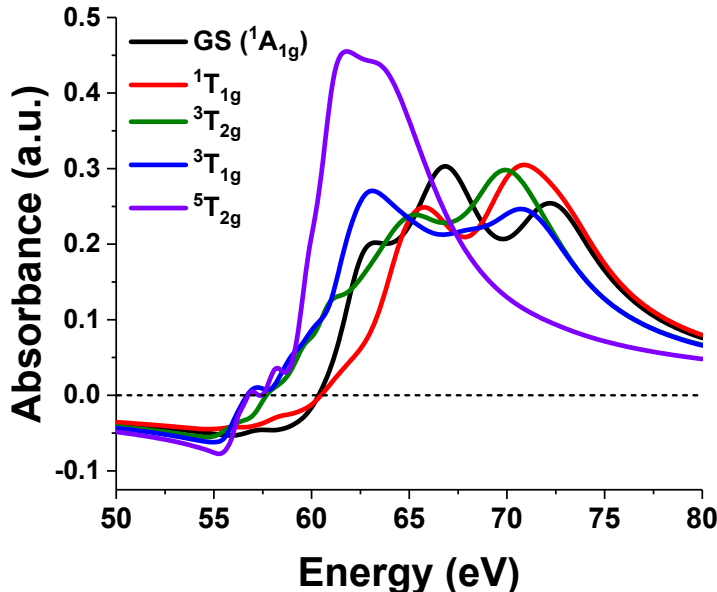


**Figure S9.** Raw (unsubtracted) LFM simulations.

## 7. DFT Summary

To support the energy ordering found using the Tanabe-Sugano diagram, density functional theory (DFT) calculations were performed using the Gaussian 16 program using the 6-311G(d) basis set with the B3LYP and MN15 functionals.<sup>12</sup> In both cases, the triplet energy is significantly below the quintet energy, consistent with the T-S prediction and the qualitative potential energy surfaces presented in the main paper. The starting geometry was taken from crystal structure,<sup>1</sup> and optimized into the lowest energy singlet, triplet, and quintet states. All calculations were performed from this initial geometry except the quintet in B3LYP, which resulted in a delocalized local minimum structure where the spin density is equally shared between two adjacent cobalt atoms. That calculation was repeated starting from the triplet geometry, resulting in the lower energy (by 0.47 eV) localized quintet reported below.

Bond lengths and energies from the calculations are summarized in Table S6, with coordinates for all optimized geometries reported in the following section. The calculated energies differ between

functionals but are consistent in predicting the same state ordering of singlet < triplet < quintet. Bond lengths are reported with respect to a single cobalt center within Co<sub>4</sub>O<sub>4</sub>; in the triplet and quintet structures this is the one upon which the spin density localizes, whereas in the singlet all are nominally equivalent. Bond lengths are seen to expand with increasing multiplicity and, in concert with the state orderings, are consistent with the qualitative schematic proposed in Figure 5 of the main text.

	Functional	Singlet	Triplet	Quintet
<b>Energy (Hartrees)</b>	B3LYP	-7739.963389	-7739.936488	-7739.927891
	MN15	-7738.455619	-7738.435054	-7738.412874
<b>Relative Energy (eV)</b>	B3LYP	0	0.73	0.97
	MN15	0	0.56	1.16
<b>Average Co-O Distance (Å)</b>	B3LYP	1.906	1.978	2.004
	MN15	1.874	1.978	1.969
<b>Co-N Distance (Å)</b>	B3LYP	1.991	1.997	2.157
	MN15	1.936	1.946	2.118

**Table S6.** Parameters from DFT calculations.

## 8. DFT Geometries

Singlet		B3LYP			MN15		
Center Number	Atomic Number	X (Å)	Y (Å)	Z (Å)	X (Å)	Y (Å)	Z (Å)
1	27	0.910782	1.100041	0.905125	-0.89831	-1.39076	-0.07119
2	27	0.91713	-1.09463	-0.90992	-0.90442	1.390816	0.065046
3	8	0.937879	0.775823	-0.93463	-0.93092	0.052723	-1.20535
4	8	0.943363	-0.77056	0.929916	-0.93519	-0.05278	1.199204
5	8	0.735361	1.137601	2.868336	-0.77026	-2.71367	1.320457
6	8	0.74097	-1.13333	-2.87286	-0.77641	2.714154	-1.32605
7	8	-0.72841	2.868088	-1.14352	0.775928	-1.32329	-2.71152
8	8	0.717089	3.030501	0.604947	-0.70003	-2.60417	-1.55589
9	7	2.879466	1.373359	1.018201	-2.82441	-1.58708	-0.10769
10	7	2.887808	-1.3557	-1.02507	-2.83218	1.580153	0.092187
11	6	-0.00825	-0.33141	-3.50256	-0.04609	2.542729	-2.34046
12	6	-0.00852	0.331005	3.498383	-0.04408	-2.53951	2.337364
13	6	3.505575	1.920857	-0.03462	-3.46774	-1.84382	-1.25149
14	1	2.883416	2.070824	-0.90764	-2.84205	-1.89899	-2.13361
15	6	4.856312	2.242934	-0.00513	-4.84128	-2.03381	-1.29203
16	1	5.321363	2.685785	-0.87834	-5.32793	-2.25132	-2.23613
17	6	5.584965	1.991256	1.153383	-5.56573	-1.93169	-0.10982
18	1	6.640434	2.23774	1.208066	-6.64228	-2.07258	-0.1086
19	6	4.93288	1.418711	2.240836	-4.8911	-1.64151	1.070681
20	1	5.457395	1.204967	3.165095	-5.41924	-1.54103	2.012225
21	6	3.579296	1.12424	2.133383	-3.51298	-1.47966	1.032854
22	1	3.013447	0.699666	2.951147	-2.91684	-1.23607	1.906122
23	6	3.584504	-1.10335	-2.1415	-3.51412	1.464098	-1.05155
24	1	3.01492	-0.68306	-2.95887	-2.91209	1.219664	-1.92055
25	6	4.939738	-1.38957	-2.25066	-4.89287	1.618256	-1.09755
26	1	5.461535	-1.17346	-3.1759	-5.41521	1.510708	-2.04155

27	6	5.597011	-1.95691	-1.16364	-5.57565	1.909396	0.077977
28	1	6.653905	-2.19689	-1.21963	-6.65299	2.043882	0.070361
29	6	4.871684	-2.21168	-0.00371	-4.85806	2.021513	1.263448
30	1	5.340893	-2.65047	0.869333	-5.35085	2.241339	2.203819
31	6	3.519049	-1.89803	0.027321	-3.48324	1.839623	1.230968
32	1	2.899469	-2.04993	0.901814	-2.86249	1.906501	2.115685
33	6	-0.01428	3.502716	-0.31381	0.065449	-2.35008	-2.52952
34	6	-0.06343	5.017574	-0.41186	0.16239	-3.41485	-3.59741
35	1	-0.83227	5.390887	0.271723	1.067001	-4.00386	-3.42192
36	1	-0.32429	5.32969	-1.42272	0.251138	-2.95349	-4.5812
37	1	0.889337	5.45198	-0.1086	-0.69682	-4.08337	-3.5559
38	8	-0.73219	-0.59443	3.026809	0.70324	-1.55408	2.600625
39	8	-0.73734	0.589559	-3.03064	0.705915	1.560181	-2.60113
40	27	-0.90282	-0.92018	1.088726	0.892291	-0.06426	1.391332
41	27	-0.909	0.914206	-1.09264	0.896895	0.071375	-1.39114
42	8	-0.93027	-0.93056	-0.78007	0.923728	1.205799	0.05261
43	8	-0.93588	0.924749	0.776196	0.92928	-1.19867	-0.05237
44	8	0.737247	-3.02638	-0.60717	-0.71954	2.601072	1.554545
45	8	-0.7085	-2.87236	1.141849	0.758577	1.326304	2.714154
46	7	-2.8738	-1.17831	1.247047	2.820103	-0.08828	1.588901
47	7	-2.88208	1.159792	-1.25096	2.825555	0.104437	-1.58178
48	6	-3.50184	-1.86379	0.279418	3.50048	1.055201	1.459862
49	1	-2.88055	-2.12745	-0.56731	2.897422	1.919477	1.201393
50	6	-4.8516	-2.18212	0.356711	4.878609	1.105789	1.617736
51	1	-5.31833	-2.73858	-0.44791	5.399555	2.049239	1.499111
52	6	-5.57711	-1.78029	1.474132	5.562682	-0.06428	1.927468
53	1	-6.63182	-2.01933	1.56486	6.639546	-0.05272	2.065467
54	6	-4.92232	-1.06875	2.474356	4.846805	-1.24929	2.053875
55	1	-5.4435	-0.7375	3.365275	5.340349	-2.18555	2.289042
56	6	-3.56989	-0.7881	2.323572	3.47248	-1.22185	1.866921
57	1	-3.00011	-0.26312	3.078015	2.853077	-2.10655	1.945791
58	6	-3.57523	0.766666	-2.32833	3.473293	1.241399	-1.85686
59	1	-3.00179	0.246558	-3.08337	2.849844	2.123065	-1.93759
60	6	-4.92943	1.038668	-2.47921	4.848189	1.275851	-2.03855
61	1	-5.44805	0.705333	-3.37084	5.337842	2.214717	-2.27144
62	6	-5.58934	1.744255	-1.47817	5.569627	0.094538	-1.90965
63	1	-6.64557	1.976438	-1.56893	6.647067	0.088515	-2.04341
64	6	-4.86696	2.148869	-0.35971	4.89034	-1.07906	-1.60269
65	1	-5.33781	2.700644	0.445739	5.415718	-2.01978	-1.48198
66	6	-3.51519	1.839388	-0.28253	3.511406	-1.03544	-1.45036
67	1	-2.89627	2.104822	0.565367	2.912055	-1.90274	-1.19347
68	6	0.022543	-3.50182	0.322723	0.028571	2.340585	2.539993
69	6	0.070612	-5.00969	0.498351	0.023258	3.350365	3.664188
70	1	0.82549	-5.25361	1.252295	-0.65975	3.001539	4.444204
71	1	0.34836	-5.49787	-0.43529	-0.31735	4.321406	3.307163
72	1	-0.88849	-5.38345	0.857544	1.016343	3.425702	4.107654
73	6	-0.06535	0.514384	5.005753	-0.04212	-3.66349	3.347436
74	1	-0.88455	1.199209	5.247077	0.649967	-4.43891	3.006287
75	1	-0.26092	-0.43643	5.501494	0.286252	-3.30398	4.32181
76	1	0.857391	0.958824	5.378648	-1.03293	-4.11351	3.412694
77	6	-0.06479	-0.51529	-5.00984	-0.04513	3.666664	-3.35056

78	1	-0.87951	-1.20565	-5.25054	0.640568	4.446088	-3.00568
79	1	-0.26696	0.434162	-5.50554	0.290332	3.309018	-4.32319
80	1	0.860676	-0.95358	-5.38328	-1.03818	4.110946	-3.42109

Center Number	Atomic Number	Triplet			MN15		
		B3LYP X (Å)	B3LYP Y (Å)	B3LYP Z (Å)	MN15 X (Å)	MN15 Y (Å)	MN15 Z (Å)
1	27	-0.92098	0.574462	-1.39423	-0.89473	0.794472	1.16691
2	27	-0.89255	-0.55875	1.348535	-0.90835	-0.83139	-1.22771
3	8	-0.95148	1.108022	0.527419	-0.94404	-0.97958	0.700109
4	8	-0.94151	-1.14572	-0.41486	-0.941	1.050127	-0.64261
5	8	-0.77219	-0.53549	-3.11637	-0.69645	2.697015	1.439606
6	8	-0.69451	0.327579	3.104818	-0.73635	-2.83962	-1.30647
7	8	0.715031	3.108895	-0.25289	0.76798	-1.37253	2.674742
8	8	-0.74599	2.52637	-1.88264	-0.73394	0.294742	3.023944
9	7	-2.89284	0.778753	-1.63369	-2.82013	0.906282	1.328645
10	7	-2.85896	-0.76193	1.590462	-2.84497	-0.93318	-1.39073
11	6	0.031618	1.350303	3.260682	0.003456	-3.49667	-0.52226
12	6	-0.02111	-1.54686	-3.23359	0.047211	3.393444	0.696477
13	6	-3.53208	1.623891	-0.80921	-3.49039	-0.16078	1.777071
14	1	-2.91295	2.05056	-0.02873	-2.87507	-1.03203	1.97751
15	6	-4.88726	1.895782	-0.94338	-4.86973	-0.14088	1.934263
16	1	-5.36622	2.583476	-0.25617	-5.38273	-1.02528	2.295263
17	6	-5.60294	1.27669	-1.96376	-5.56485	1.023816	1.628161
18	1	-6.66213	1.473647	-2.09462	-6.64246	1.07135	1.752749
19	6	-4.93471	0.401841	-2.8145	-4.85898	2.124846	1.156446
20	1	-5.44919	-0.10091	-3.62532	-5.36136	3.050995	0.900337
21	6	-3.57739	0.178946	-2.61802	-3.483	2.022754	1.009627
22	1	-2.99344	-0.47348	-3.25418	-2.87056	2.83611	0.640487
23	6	-3.5472	-0.08955	2.523117	-3.52714	-2.05191	-1.12152
24	1	-2.96843	0.611509	3.109183	-2.92499	-2.90476	-0.83379
25	6	-4.90297	-0.3026	2.74123	-4.90888	-2.10814	-1.22988
26	1	-5.41825	0.260571	3.510996	-5.42828	-3.03455	-1.01278
27	6	-5.56877	-1.24686	1.965954	-5.59736	-0.96336	-1.6145
28	1	-6.62635	-1.4393	2.115614	-6.67917	-0.97518	-1.70575
29	6	-4.85056	-1.94205	0.997704	-4.88035	0.198536	-1.8758
30	1	-5.32621	-2.68723	0.370403	-5.37903	1.116485	-2.16555
31	6	-3.49676	-1.67371	0.84	-3.49813	0.176594	-1.75548
32	1	-2.87688	-2.15743	0.094687	-2.86828	1.046252	-1.91372
33	6	-0.00484	3.344665	-1.2624	0.024068	-0.64279	3.392362
34	6	0.004328	4.767778	-1.79234	0.080105	-0.90678	4.879359
35	1	0.30827	4.764419	-2.84191	0.808861	-0.22545	5.327812
36	1	0.676352	5.39852	-1.2127	0.396078	-1.9307	5.075431
37	1	-1.00848	5.176389	-1.75378	-0.88899	-0.70359	5.335107
38	8	0.737554	-2.04273	-2.35427	0.762907	3.008443	-0.27194
39	8	0.766657	1.925604	2.404121	0.737087	-3.03792	0.39335
40	27	0.903283	-1.323	-0.52704	0.884311	1.161538	-0.7761
41	27	0.894147	1.320094	0.543375	0.882949	-1.15289	0.777756

42	8	0.950173	-0.45035	1.116066	0.888826	-0.68452	-1.02431
43	8	0.898694	0.466096	-1.14352	0.932035	0.668092	0.988658
44	8	-0.67871	-2.40722	1.987775	-0.77048	-0.15057	-3.07992
45	8	0.765255	-3.05887	0.356519	0.749846	1.47376	-2.67385
46	7	2.884819	-1.58382	-0.58339	2.82076	1.298831	-0.89838
47	7	2.872814	1.616914	0.532897	2.815036	-1.32545	0.852568
48	6	3.527116	-1.78436	0.577254	3.474021	0.576487	-1.81334
49	1	2.913775	-1.67471	1.462342	2.853748	-0.09544	-2.3969
50	6	4.882196	-2.0849	0.629976	4.849064	0.672856	-1.97561
51	1	5.359926	-2.24185	1.590213	5.347072	0.0678	-2.7249
52	6	5.598652	-2.18197	-0.55893	5.559804	1.551312	-1.16565
53	1	6.657102	-2.42151	-0.54963	6.635066	1.654177	-1.27513
54	6	4.930329	-1.96734	-1.7601	4.872647	2.293101	-0.21144
55	1	5.444832	-2.03255	-2.71201	5.388491	2.984167	0.445708
56	6	3.573369	-1.67049	-1.72947	3.499314	2.13082	-0.10189
57	1	2.997109	-1.51676	-2.63124	2.901797	2.667252	0.624922
58	6	3.589237	1.706162	1.66156	3.463506	-2.17023	0.044537
59	1	3.037005	1.537092	2.575676	2.844303	-2.69684	-0.67137
60	6	4.942094	2.02324	1.658902	4.835963	-2.35375	0.125844
61	1	5.479956	2.090175	2.597682	5.327501	-3.0535	-0.54066
62	6	5.576235	2.255019	0.442613	5.553751	-1.62092	1.064595
63	1	6.630634	2.509524	0.40768	6.629206	-1.74092	1.152697
64	6	4.830837	2.15533	-0.72822	4.873843	-0.72911	1.886141
65	1	5.281372	2.324921	-1.69939	5.396817	-0.13059	2.62357
66	6	3.482065	1.835332	-0.64202	3.49751	-0.60995	1.751327
67	1	2.849458	1.724379	-1.51345	2.89801	0.073547	2.342788
68	6	0.041832	-3.24778	1.379802	0.003873	0.789149	-3.42268
69	6	0.021155	-4.66737	1.9194	0.021911	1.12484	-4.89533
70	1	-0.73163	-5.242	1.370917	-0.98722	1.392691	-5.2159
71	1	-0.24565	-4.67348	2.975825	0.314958	0.238836	-5.46298
72	1	0.985623	-5.15118	1.76329	0.707063	1.945821	-5.09959
73	6	-0.05385	-2.25488	-4.57778	0.125649	4.868205	1.019078
74	1	-0.00355	-1.52499	-5.38781	0.998788	5.041337	1.655235
75	1	0.758047	-2.9758	-4.66379	0.254233	5.449166	0.105848
76	1	-1.00418	-2.78788	-4.6766	-0.76001	5.19066	1.56584
77	6	-0.00131	1.987564	4.639775	-0.01927	-4.99993	-0.67669
78	1	-0.18307	1.234037	5.406159	-0.08865	-5.26901	-1.73111
79	1	0.924373	2.525879	4.843195	0.858789	-5.45096	-0.216
80	1	-0.82112	2.712197	4.67324	-0.9089	-5.38909	-0.17286

Quintet		B3LYP			MN15		
Center Number	Atomic Number	X (Å)	Y (Å)	Z (Å)	X (Å)	Y (Å)	Z (Å)
1	27	-0.99801	0.708023	-1.24463	-0.8141	-0.22715	-1.45314
2	27	-0.8117	-0.82256	1.291154	-0.94456	0.306815	1.387505
3	8	-0.9358	0.947439	0.746927	-0.91463	1.186007	-0.27589
4	8	-0.9333	-1.08548	-0.55045	-0.92483	-1.19922	0.089349
5	8	-0.91883	-0.13527	-3.14394	-0.5822	-1.83749	-2.47723

6	8	-0.56085	-0.25888	3.153137	-0.84101	2.135768	2.282315
7	8	0.659977	3.101976	0.274608	0.821711	2.385409	-1.82597
8	8	-0.84668	2.755286	-1.37689	-0.61469	1.00868	-2.91754
9	7	-3.11141	1.050316	-1.50876	-2.73904	-0.252	-1.68958
10	7	-2.76764	-1.07405	1.558775	-3.04726	0.293331	1.645013
11	6	0.163723	0.732492	3.460405	-0.01219	3.008913	1.898745
12	6	-0.12368	-1.07109	-3.44077	0.138914	-2.78785	-2.05856
13	6	-3.73486	1.738871	-0.54197	-3.41483	0.898701	-1.59167
14	1	-3.1132	2.005361	0.305611	-2.80339	1.771178	-1.38613
15	6	-5.08145	2.071893	-0.62273	-4.79769	0.944139	-1.7048
16	1	-5.54981	2.628947	0.180587	-5.31422	1.89267	-1.6101
17	6	-5.80285	1.68064	-1.74739	-5.49159	-0.23693	-1.94261
18	1	-6.85499	1.929857	-1.84201	-6.57271	-0.23017	-2.04341
19	6	-5.15237	0.967443	-2.74998	-4.78005	-1.427	-2.04435
20	1	-5.67532	0.647003	-3.64388	-5.2809	-2.37125	-2.22664
21	6	-3.80295	0.671909	-2.59142	-3.40017	-1.39458	-1.90123
22	1	-3.2322	0.130838	-3.33689	-2.78321	-2.28267	-1.96192
23	6	-3.43785	-0.4847	2.55823	-3.75753	1.376692	1.97226
24	1	-2.84684	0.156889	3.197222	-3.17676	2.275532	2.150721
25	6	-4.79339	-0.70312	2.771671	-5.14088	1.340491	2.088395
26	1	-5.29363	-0.20924	3.596871	-5.68618	2.237049	2.361324
27	6	-5.47906	-1.56188	1.918181	-5.79722	0.137039	1.854128
28	1	-6.53722	-1.75575	2.061262	-6.87795	0.074455	1.939418
29	6	-4.78083	-2.16724	0.877904	-5.05166	-0.98517	1.509208
30	1	-5.27278	-2.84115	0.186027	-5.52751	-1.939	1.310181
31	6	-3.42588	-1.89926	0.730394	-3.67172	-0.86607	1.413309
32	1	-2.82819	-2.31511	-0.0705	-3.02055	-1.68863	1.128948
33	6	-0.11192	3.483681	-0.64824	0.111812	2.032543	-2.8123
34	6	-0.1728	4.977561	-0.91376	0.172548	2.931089	-4.02586
35	1	0.087194	5.173121	-1.95696	0.877506	2.502559	-4.74417
36	1	0.500875	5.522801	-0.25467	0.513427	3.928092	-3.75004
37	1	-1.19662	5.33087	-0.76745	-0.80339	2.974225	-4.50989
38	8	0.710763	-1.63473	-2.67567	0.824691	-2.83579	-1.00116
39	8	0.825109	1.483551	2.687644	0.798424	2.913292	0.939185
40	27	0.933351	-1.20298	-0.76601	0.901615	-1.37581	0.246115
41	27	0.911783	1.211605	0.733502	0.935888	1.365322	-0.2012
42	8	1.016603	-0.63058	1.00086	0.964369	0.186596	1.248574
43	8	0.946846	0.665064	-1.07085	1.001154	-0.19115	-1.15637
44	8	-0.55211	-2.74873	1.589522	-0.87972	-1.14228	2.790343
45	8	0.832521	-3.07348	-0.18361	0.647425	-2.48247	1.805651
46	7	2.893696	-1.40955	-0.91776	2.823827	-1.57923	0.386859
47	7	2.881834	1.571015	0.74	2.856092	1.534741	-0.1951
48	6	3.581762	-1.80757	0.162554	3.411933	-1.66167	1.584639
49	1	2.998056	-1.895	1.069419	2.747332	-1.57051	2.434692
50	6	4.947004	-2.05883	0.115698	4.779485	-1.8522	1.716648
51	1	5.464028	-2.38026	1.012439	5.221259	-1.926	2.704008
52	6	5.622652	-1.89341	-1.08934	5.557004	-1.93575	0.566788
53	1	6.688077	-2.0881	-1.1578	6.630591	-2.08205	0.636358
54	6	4.905276	-1.47313	-2.20485	4.939541	-1.82382	-0.67371
55	1	5.387449	-1.32912	-3.16493	5.510329	-1.87024	-1.59437
56	6	3.541787	-1.23967	-2.07788	3.563085	-1.64935	-0.72337

57	1	2.928669	-0.92879	-2.91192	3.01017	-1.53966	-1.6503
58	6	3.6199	1.532643	1.857555	3.503365	1.603604	0.972131
59	1	3.093371	1.225106	2.750353	2.874701	1.502392	1.850029
60	6	4.961184	1.895436	1.87482	4.881173	1.761128	1.031771
61	1	5.517368	1.852045	2.804298	5.376044	1.808036	1.995291
62	6	5.559135	2.316626	0.691474	5.598655	1.855087	-0.15533
63	1	6.603183	2.612544	0.673508	6.6763	1.986293	-0.13852
64	6	4.790444	2.352867	-0.46786	4.915872	1.773701	-1.36361
65	1	5.212252	2.673345	-1.41362	5.436676	1.834386	-2.31255
66	6	3.455965	1.972383	-0.40414	3.539524	1.603219	-1.34219
67	1	2.804299	1.950193	-1.26849	2.944317	1.52136	-2.24277
68	6	0.157661	-3.4545	0.817872	-0.16337	-2.17956	2.722746
69	6	0.184124	-4.94592	1.104268	-0.29138	-3.15609	3.867759
70	1	-0.56379	-5.43949	0.476026	-1.33144	-3.47994	3.947749
71	1	-0.05949	-5.14227	2.147894	-0.03987	-2.6506	4.802888
72	1	1.157369	-5.36695	0.850607	0.355633	-4.01921	3.720476
73	6	-0.18884	-1.58938	-4.86746	0.158128	-4.03268	-2.91497
74	1	-0.1764	-0.75289	-5.56908	1.132476	-4.5178	-2.85627
75	1	0.632106	-2.27317	-5.0784	-0.58512	-4.73477	-2.52575
76	1	-1.13435	-2.12034	-5.01111	-0.09555	-3.79245	-3.94683
77	6	0.280371	1.038501	4.944305	-0.01532	4.31999	2.649049
78	1	1.153747	0.514733	5.345746	-0.16056	4.141695	3.715091
79	1	0.423929	2.107093	5.10478	0.906214	4.871845	2.46944
80	1	-0.59658	0.68355	5.485518	-0.85589	4.922966	2.293829

## 9. References

- 1 R. Chakrabarty, S. J. Bora and B. K. Das, *Inorg. Chem.*, 2007, **46**, 9450–9462.
- 2 Y. Shari’ati and J. Vura-Weis, .
- 3 K. Zhang, M. F. Lin, E. S. Ryland, M. A. Verkamp, K. Benke, F. M. F. De Groot, G. S. Girolami and J. Vura-Weis, *J. Phys. Chem. Lett.*, 2016, **7**, 3383–3387.
- 4 J. Vura-Weis, C. M. Jiang, C. Liu, H. Gao, J. M. Lucas, F. M. F. De Groot, P. Yang, A. P. Alivisatos and S. R. Leone, *J. Phys. Chem. Lett.*, 2013, **4**, 3667–3671.
- 5 P. Andersen, T. Andersen, F. Folkmann, K. Ivanov V, H. Kjeldsen and J. B. West, *J. Phys. B At. Mol. Opt. Phys.*, 2001, **34**, 2009–2019.
- 6 H. Wang, A. T. Young, J. Guo, S. P. Cramer, S. Friedrich, A. Braun and W. Gu, *J. Synchrotron Radiat.*, 2013, **20**, 614–619.
- 7 S. G. Chiuzăian, G. Ghiringhelli, C. Dallera, M. Grioni, P. Amann, X. Wang, L. Braicovich and L. Patthey, *Phys. Rev. Lett.*, 2005, **95**, 197402.
- 8 K. Zhang, R. Ash, G. S. Girolami and J. Vura-Weis, *J. Am. Chem. Soc.*, 2019, **141**, 17180–17188.
- 9 D. Nicholls, *The chemistry of iron, cobalt and nickel*, Pergamon Press, 1973.
- 10 E. Stavitski and F. M. F. de Groot, *Micron*, 2010, **41**, 687–694.

- 11 K. Zhang, G. S. Girolami and J. Vura-Weis, *J. Synchrotron Radiat.*, 2018, **25**, 1600–1608.
- 12 H. S. Yu, X. He, S. L. Li and D. G. Truhlar, *Chem. Sci.*, 2016, **7**, 5032–5051.